Int. j. adv. multidisc. res. stud. 2024; 4(5):170-178

Received: 22-07-2024
Accepted: 02-09-2024

International Journal of Advanced Multidisciplinary Research and Studies

ISSN: 2583-049X

Computer Simulation of Deformation characteristics of Hybrid Orthotropic Composite Sandwich Beams Under Bending and Axial Loading

[1] Umar Farooq, [2] Peter Myler, [3] Mamadou Ndiaye, [4] Sadia Sattar, [5] Faraht Imtiaz, [6] Mamoona Siddique

[1] Reader, Faculty of Engineering, Support and Advance Sciences, University of Bolton, Bolton BL3 5AB, United Kingdom
[2] Professor, Faculty of Engineering, Support and Advance Sciences, University of Bolton, Bolton BL3 5AB, United Kingdom
[3] Program Leader, Faculty of Engineering, Support and Advance Sciences, University of Bolton, Bolton BL3 5AB, United Kingdom
[4] Assistant Professor, Department of Mathematics, Ghazi University, Dera Ghazi Khan, Pakistan
[5] Assistant Professor, Department of Mathematics, Govt Degree College for Women, Sargodha Pakistan
[6] Lecturer, Department of Mathematics and Statistics, University of Lahore (Sargodha Campus), Pakistan

DOI: https://doi.org/10.62225/2583049X.2024.4.5.3211
Corresponding Author: **Umar Farooq**

Abstract

This study focuses on the deformation characteristics of hybrid orthotropic composite sandwich beams under axial and bending loading. The homogeneous cores of the hybrid orthotropic sandwich beams affect different parameters on structures. We followed by analytically determining effective material properties to study response of the hybrid sandwich beam under axial and bending loading. Ensuing, we programmed all steps and procedures of solution algorithm into commercially available MATLAB™ 2020 code to simulate practical scenarios. Subsequently, we collected and processed data in tabular and graphical forms to facilitate analyses. We compared simulation generated results to the data results available in the literature and found to be within the acceptable range of (±6%) deviations. We observed that the hybrid structure beams had undergone less deformation that confirmed that the hybrid structure beams have comprehensive mechanical advantages as well as has high strength and specific energy absorption capabilities. Based on comparison of the results, the hybrid beams are more damage resistant and tolerant than beams made of the other type of materials. Since hybrid sandwich beams are relatively light, economical, and perform better under axial and bending deformations. Therefore, this study could also be extended to investigate performance of the orthotropic sandwich beam structures under multiple loading directions as well as proposes that the usage of the hybrid sandwich beam components will be useful in global structures.

Keywords: Hybrid Structures, Honeycomb Structures, High Shear Deformation Theory, Finite Elements Analysis, and Orthotropic Beam

1. Introduction

Owing to the exceptional properties, applications of the hybrid orthotropic beam structures are growing at a huge rate in automobile, railroad, civil, aeronautical, sports, military, health, and marine industry. Accordingly, the hybrid structures have attracted attention of the researchers for safer and economical widespread applications. The goal of the current study is to develop a simulation model on hybrid orthotropic sandwich beams of mixed material properties under axial and bending loading. A brief literature review of the previous relevant work on the topic is presented below.

The study of sandwich structure and deformation characteristics of sandwich beams is given in [1]. Interest in sandwich laminate structures, deformation capability, and performance is much better when compared to classical laminates was claimed in [2]. An increase in the thickness of honeycomb foam cores provides higher stiffness and strength of the panel at the minimum addition of weight sandwich structures in several applications. Such cores demonstrate higher fatigue strength, better acoustical, and thermal insulation. Equally, usage of honeycomb cores has demonstrated high crushing strength, stiffness, fatigue, and moisture advantages over the foam and wood-based sandwich structures reported in [3]. Strength analyses on honeycomb sandwich panels of different materials and deformation behaviour of Aluminium honeycomb sandwich panels are presented in [4]. The sandwich structures allow simplified analyses and mathematical accuracy with size effects of basic cell in static analyses were studied in

[5]. The extent of damage determined for structural components by suitable non-destructive test(NDT) methods was confirmed in [6] and [7]. Alternatively, the damaged areas can be located by simply tapping the surface and listening to the sound. Nonetheless, the damaged areas give a dull response to the tapping, and the boundary between while it can easily be mapped to identify the area for repair was reported in [8]. To certain extend damage can be controlled according to the Aircraft Structural Repair Manual guided in [9], [10]. Advances in materials processing and fabrication techniques including digital manufacturing of hybrid sandwich beams were detailed in [11] and [12].

Sandwich composite structures offer a very high stiffness-to-weight ratio, high strength composite skins, and separated by and bonded to a light weight honeycomb or foam cores was proposed in [13]. A hybrid sandwich panel enhances flexural rigidity of the structure without adding substantial weight was illustrated in [14]. Parts of the aircrafts like ailerons, flaps and rudders manufactured from honeycomb sandwich panels are explained in [15] and [16]. Early theoretical work restricted to uniform lateral loading and simply supported boundary conditions was described in [17, 18]. Understanding failure modes and analytical study for three-point bend test are provided in [19]. Sandwich construction steady increasing in satellites, large aircrafts for the global range transport, and navies' ship hulls reported in [20] and [21]. The usage of different shapes of core combination produces hybrid core with special characteristics were discussed in [22] and [23]. The advantages relative to the Classical Beam Theory and First-Order Shear Deformation Theory were analysed in [24]. Theoretical results were compared and validated with experimentally and finite element produced numerical quantities in [26] and [27]. The guide to give a general approach to sandwich composite beam repair in all applications is provided in [28]. Flexural deformations as well as vibration response of fibre-metal composite sandwich panels using different analytical models, numerical techniques, and experimental methods were presented in [28].

The review of previous studies revealed that a great deal of experimental and theoretical research work is available on orthotropic hybrid composite sandwich beams. Nonetheless, majority of the researchers exploited expensive and time consuming experimental and analytical methods. The sandwich structures are formed by materials with very different resistance in the faces and in the core. The materials' heterogeneities do not fit-in the classical beam deformation theories. On the other hand, the range of applications is expanding in marine structures, high speed craft, and blast loading resistant structures. Therefore, their study poses persistent challenge for researchers in the field.

The current study is another effort to complement the researchers in resolving the much needed gap. The proposed study is based on analytical determination of material properties and simulation modelling of hybrid beams under axial and bending loading.

2. Materials and Methods

2.1 Hybrid Sandwich Materials

A hybrid sandwich structure consists of two thin face sheets attached to both sides of a lightweight core. The design of sandwich structures allows the outer face sheets to carry the axial loads, deformation moments, and in-plane shears while the core carries the normal flexural shears. Sandwich structures are susceptible to failures due to large normal local stress concentrations because of the heterogeneous nature of the core and face-sheets' assembly. Mounting of components must therefore be sealed inserts to distribute loads from connections. The face-sheets are commonly fabricated using metals like aluminium, steel or graphite/epoxy composite panels. The core is typically fabricated using foam, honeycomb or aluminium construction. The orthotropic hybrid sandwich beam structure considered for this study has length (L), width (W=b) and thickness ($h_0 = H$ is). It is referred to a Cartesian co-ordinate system: $x_1, x_2, x_3 (0 \leq x_1 \leq L, 0 \leq x_2 \leq b, -H/2 \leq x_3 \leq H/2)$. We assumed symmetric beams with respect to the mid-plane $x_3 = 0$, with the face thickness h_f and the core thickness $H_I = 2h_c$. The dimension of the beam sets may vary: (for example, 1m, width to 0.1m, and the height to 0.27m). They are subjected to axial as well as deformation loading while boundaries may be simply or free-fixe supported on four edges. The beams are free to expand/retract in x- and y-direction along two sides. The boundary condition is assigned along while using solid elements to ensure a good transfer of the support force to the three layers without the risk of local distortion that may corrupt the result. Transformations of parameters are related to Fig 1. The first step transforms the sandwich structure to a three layered beam mainly done by loading the structure in different ways and measuring displacements. The first transformation is an equivalent stiffness of the core obtained from simple equations that treat shear and flexural deflection. The second part translates the three layers into one layer. The second transformation, however, is derived analytically from assumptions regarding the behaviour and equilibrium of a three-layered sandwich beam.

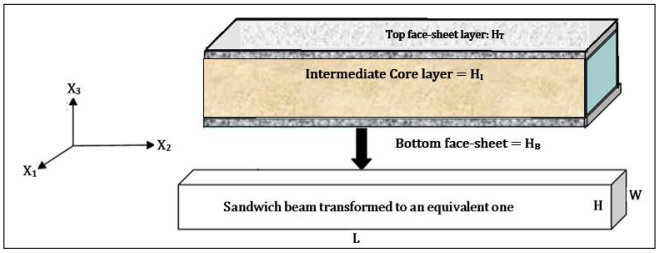

Fig 1: Schematic of sandwich-beam to an equivalent one layered-beam

2.2 Derivation of one equivalent property of a 3-layer sandwich beam

This section describes analytical solutions for isotropic and orthotropic beams to determine elastic properties. Since stiffness parameters of sandwich structures deform according to applied loading, so we study performance behaviour of the structures through changes in the stiffness parameters. This is followed by establishing different ways of transforming a multi-layered structure into an equivalent one-layer. We applied two different transformation methods for establishing the equivalent Young's moduli of Fig 2: (a) axial loaded and (b) flexural rigidity based deformations. Transformations are performed for nine deferent elastic parameters: 3 Young's, 3 shear moduli, and 3 Poisson's ratios. No interaction between the different parameters is assumed. We transformed the elastic moduli by assuming E_{11} and E_{22} as on axial load deformation or constant flexural rigidity. We also assume no flexural in z-direction transformation, since the elastic modulus in z-direction inherits low height to length ratio.

2.2.1 Equivalent Young's moduli under axial-compressive loads

For determining the in-plane Young's modulus E_{11} and E_{22}, the setup of the beam and axial loading used is depicted in Fig 2.

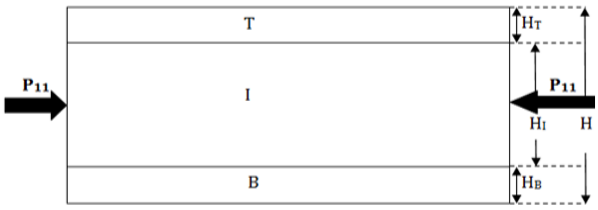

Fig 2: Axial loading in x-direction and transformation in y-direction

Load is applied in x-direction (direction 1) and uniformly distributed among all layers: T-top, I-interface, and B-bottom layer. We determine Young's moduli from relationships of applied loading and stresses as follows:

$$\begin{cases} P_{11} = P_{11}^T + P_{11}^I + P_{11}^B \\ \sigma_{11}.A_{11} = \sigma_{11}^T.A_{11}^T + \sigma_{11}^I.A_{11}^I + \sigma_{11}^B.A_{11}^B \\ \sigma_{11} \Rightarrow \sigma_{11}^T.\frac{A_{11}^T}{A_{11}} + \sigma_{11}^I.\frac{A_{11}^I}{A_{11}} + \sigma_{11}^B.\frac{A_{11}^B}{A_{11}} \\ where : \\ A_{11} = H.W, \quad A_{11}^T = H^T.W \quad A_{11}^I = H^I.W, A_{11}^B = H^B.W \end{cases} \quad (1)$$

Whereas:

$$\begin{cases} \alpha_T = \frac{H_T}{H} \quad \alpha_I = \frac{H_I}{H} \quad \alpha_B = \frac{H_B}{H} \\ Put \quad in \quad (1) \\ \sigma_{11} = \sigma_{11}^T.\alpha_T + \sigma_{11}^I.\alpha_I + \sigma_{11}^B.\alpha_B \\ Divide \quad by \quad \varepsilon_{11}: \\ \frac{\sigma_{11}}{\varepsilon_{11}} = \frac{\sigma_{11}^T}{\varepsilon_{11}}.\alpha_T + \frac{\sigma_{11}^I}{\varepsilon_{11}}.\alpha_I + \frac{\sigma_{11}^B}{\varepsilon_{11}}.\alpha_B \\ Gives : \\ E_{11} = E_{11}^T.\alpha_T + E_{11}^I.\alpha_I + E_{11}^B.\alpha_B \\ E_{22} = E_{22}^T.\alpha_T + E_{22}^I.\alpha_I + E_{22}^B.\alpha_B \end{cases} \quad (2)$$

2.2.2 Equivalent constants based on deformation-flexural method

The computation of the equivalent moduli of E_{11} and E_{22} for the flexural method is based on flexural stiffness. The following procedure is based on the setup, which can be seen in Fig 3. The flexural stiffness of the beam is treated as a sandwich composite beam, which simplifies the theoretical analysis. In order to formulate level position of the neutral axis, the following procedure was followed.

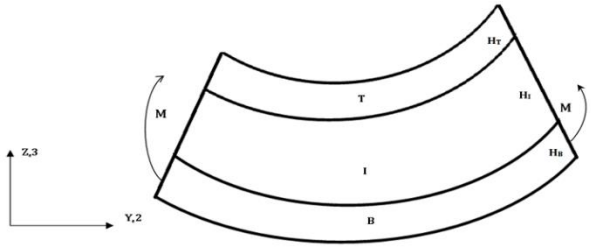

Fig 3: Assumed load and deflection for the transformation based on flexural rigidity

Likewise, we considered a three-layer sandwich structure in Fig 4 for calculations where neutral axis is situated at the shifted level.

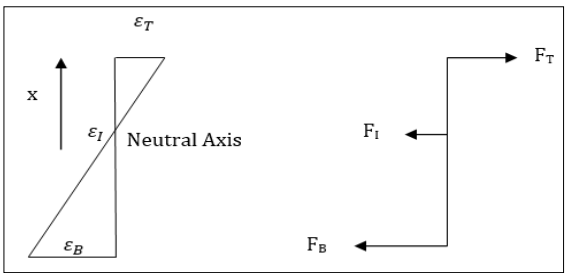

Fig 4: Strain and force equilibrium

The relation between the different strains of the 3-layer sandwich beam with height total H and width W was determined as follows:

$$\begin{cases} \frac{\varepsilon_T}{x-\frac{H_T}{2}} = \frac{\varepsilon_B}{x-H+\frac{H_B}{2}} \Rightarrow \varepsilon_B = \frac{\varepsilon_B\left(x-H+\frac{H_B}{2}\right)}{x-\frac{H_T}{2}}, \varepsilon_I = \frac{\varepsilon_T\left(x-\frac{H}{2}\right)}{x-\frac{H_T}{2}} \\ Rewrite : \\ F_T + F_I + F_B = 0 \Rightarrow (\varepsilon.E.A)_T + (\varepsilon.E.A)_I + (\varepsilon.E.A)_B = 0 \\ Insert : \\ \varepsilon_T.E_T.A_T + \frac{\varepsilon_T\left(x-\frac{H}{2}\right)}{x-\frac{H_T}{2}}.E_T.A_T + \frac{\varepsilon_T\left(x-H+\frac{H_B}{2}\right)}{x-\frac{H_T}{2}}.E_B.A_B = 0 \\ Gives : \\ x = \frac{-E_BH_B^2 + 2E_BHH_B + E_TH_T^2 + E_IHH_I}{2(E_BH_B + E_IH_I + E_TH_T)} \end{cases} \quad (3)$$

$$\begin{cases} D = D_T + D_I + D_B \\ D_T = E_{11}^T.\frac{I_{11}^T}{W} \\ I_{11}^T = W.\frac{H_T^3}{12} + W.H_T.x^2 \\ D_T = E_{11}^T\left(\frac{H_T^3}{12} + H_T.x^2\right) \\ D_I = E_{11}^I\left(\frac{H_I^3}{12} + H_I\left(x-\frac{H_T}{2}-x^2\right)^2\right) \\ D_B = E_{11}^B\left(\frac{H_B^3}{12} + H_B(H-x)^2\right) for\ single\ layer \\ D = E_{EQ}.\frac{H^3}{12} where \\ E_{EQ} = \frac{12E_T\left(\frac{H_T^3}{12} + \frac{H_T(-E_BH_B^2 + 2E_BHH_B + E_TH_T^2 + E_IHH_I)^2}{4(E_BH_B + E_IH_I + E_TH_T)^2}\right)}{H^3} \\ + \frac{12E_B\left(\frac{H_B^3}{12} + H_B\left(\frac{H - E_BH_B^2 + 2E_BHH_B + E_TH_T^2 + E_IHH_I}{2E_BH_B + 2E_IH_I + 2E_TH_T}\right)^2\right)}{H^3} \\ + \frac{12E_I\left(\frac{H_I^3}{12} + H_I\left(\frac{H_I}{2} + \frac{H_T}{2} - \frac{-E_BH_B^2 + 2E_BHH_B + E_TH_T^2 + E_IHH_I}{2E_BH_B + 2E_IH_I + 2E_TH_T}\right)^2\right)}{H^3} \end{cases} \quad (4)$$

The equation (4) can be used to express both E_{11} and E_{22}.

2.2.3 Equivalent elastic constants in z-direction

The equivalent elastic engineering modulus in z-direction can be described as compression of the beam over its thickness. This process is also used in both transformational methods, axial-compressive and flexural derived from Fig 5.

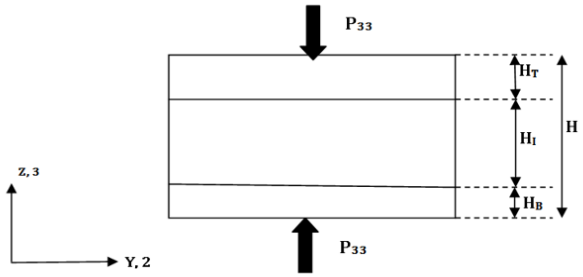

Fig 5: Assumed load in z-direction evenly distributed over the face sheet

Assume load P_{33} in z-direction is distributed over the whole bottom and top face sheets:

$$\begin{cases} \sigma_{33} = \dfrac{P_{33}}{A_{33}} & Transform: \\ \sigma_{33} = \sigma_{33}^T + \sigma_{33}^I + \sigma_{33}^B & Strains: \\ \varepsilon_{33}^T = \dfrac{\sigma_{33}^T}{E_{33}^T}, \quad \varepsilon_{33}^I = \dfrac{\sigma_{33}^I}{E_{33}^I}, \quad \varepsilon_{33}^B = \dfrac{\sigma_{33}^B}{E_{33}^B} & \end{cases} \quad (5)$$

The total displacement can be expressed by the sum of the contribution from all layers gives elastic Young's modulus in z-direction:

$$\begin{cases} \delta_{33} = \delta_{33}^T + \delta_{33}^I + \delta_{33}^B \\ : = \varepsilon_{33}^T.H^T + \varepsilon_{33}^I.H^I + \varepsilon_{33}^B.H^B \\ \varepsilon_{33} = \dfrac{\delta_{33}}{H} = \dfrac{\varepsilon_{33.H^T}^T}{H} + \dfrac{\varepsilon_{33.H^I}^I}{H} + \dfrac{\varepsilon_{33.H^B}^B}{H} \\ Dividing\ by\ \sigma_{33} \\ \dfrac{\varepsilon_{33}}{\sigma_{33}} = \dfrac{\varepsilon_{33.\alpha^T}^T}{\sigma_{33}} + \dfrac{\varepsilon_{33.\alpha^I}^I}{\sigma_{33}} + \dfrac{\varepsilon_{33.\alpha^B}^B}{\sigma_{33}} \\ Solve\ for\ E_{33} \\ \dfrac{1}{E_{33}} = \dfrac{\alpha^T}{E_{33}^T} + \dfrac{\alpha^I}{E_{33}^I} + \dfrac{\alpha^B}{E_{33}^B} \\ \Longrightarrow \\ E_{33} = \dfrac{1}{\frac{\alpha^T}{E_{33}^T} + \frac{\alpha^I}{E_{33}^I} + \frac{\alpha^B}{E_{33}^B}} \end{cases} \quad (6)$$

2.2.4 Equivalent shear moduli

Expressions of the equivalent shear moduli are obtained for both the axial-compressive and flexural methods The shear stiffness G_{12} is obtained by summation of the stiffness of the individual in Fig 6, and layers in the same manner as for E_{11} calculated from the axial loaded deflection.

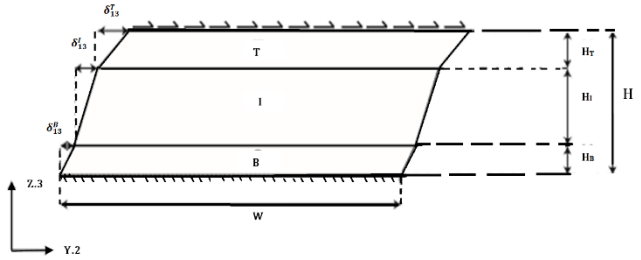

Fig 6: Shear load over top-sheet and fixed at the bottom for moduli G_{13} and G_{23}.

Expressing the shear strain and displacement for all layers according to the Fig 6, the transformation equation for calculations of shear moduli becomes:

$$\begin{cases} G_{12} = G_{12}^T.\alpha^T + G_{12}^I.\alpha^I + G_{12}^B.\alpha^B \\ \delta_{13}^T = \gamma_{13}^T.H^T, \quad \delta_{13}^I = \gamma_{13}^I.H^I, \quad \delta_{13}^B = \gamma_{13}^B.H^B \\ \delta_{13} = \delta_{13}^T + \delta_{13}^I + \delta_{13}^B = \gamma_{13}^T.H^T + \gamma_{13}^I.H^I + \gamma_{13}^B.H^B \\ \gamma_{13} = \dfrac{\delta_{13}}{H} = \gamma_{13}^T.\dfrac{H^T}{H} + \gamma_{13}^I.\dfrac{H^I}{H} + \gamma_{13}^B.\dfrac{H^B}{H} \\ \gamma_{13} = \gamma_{13}^T.\alpha_T + \gamma_{13}^I.\alpha_I + \gamma_{13}^B.\alpha_B \\ Divide\ by\ \tau_{13} \\ \dfrac{\gamma_{13}}{\tau_{13}} = \gamma_{13}^T.\alpha_T + \dfrac{\gamma_{13}^I}{\tau_{13}}.\alpha_I + \gamma_{13}^B.\alpha_B \\ \dfrac{1}{G_{13}} = \dfrac{\alpha_T}{G_{13}^T} + \dfrac{\alpha_I}{G_{13}^I} + \dfrac{\alpha_B}{G_{13}^B} \\ \Longrightarrow \\ G_{13} = \dfrac{1}{\frac{\alpha_T}{G_{13}^T} + \frac{\alpha_I}{G_{13}^I} + \frac{\alpha_B}{G_{13}^B}} \\ G_{23} = \dfrac{1}{\frac{\alpha_T}{G_{23}^T} + \frac{\alpha_I}{G_{23}^I} + \frac{\alpha_B}{G_{23}^B}} \end{cases} \quad (7)$$

2.2.5 Poisson's ratios

Poisson's ratio is a measure of how much an object expands/contracts transversely during axial loading. A positive value Poisson's ratio gives contraction, which is the normal case, and a negative one gives expansion. The following procedure is used to obtain values for both transformation methods Fig 7. Assuming loading of P_{11} in direction1, each component will then have a displacement in direction 2 that can be expressed in the relations give the desired Poisson's ratios as:

$$\begin{cases} \delta_2^T = -\nu_{12}^T.\varepsilon_{11}^T.W, \quad \delta_2^I = -\nu_{12}^I.\varepsilon_{11}^I.W, \quad \delta_2^B = -\nu_{12}^B.\varepsilon_{11}^B.W, \\ \delta_2 = \alpha_T.\delta_2^T + \alpha_I.\delta_2^I + \alpha_B.\delta_2^B \\ or = -\alpha_T.\nu_{12}^T.\varepsilon_{11}.W - \alpha_I.\nu_{12}^I.\varepsilon_{11}.W - \alpha_B.\nu_{12}^B.\varepsilon_{11}.W \\ -\nu_{12}.\varepsilon_{11}.W = -\alpha_T.\nu_{12}^T.\varepsilon_{11}^T.W - \alpha_I.\nu_{12}^I.\varepsilon_{11}^I.W - \alpha_B.\nu_{12}^B.\varepsilon_{11}^B.W \\ divide\ by\ -\varepsilon_{11} \\ \nu_{12} = -\alpha_T.\nu_{12}^T.\dfrac{\varepsilon_{11}^T}{\varepsilon_{11}} + \alpha_I.\nu_{12}^I.\dfrac{\varepsilon_{11}^I}{\varepsilon_{11}} + \alpha_B.\nu_{12}^B.\dfrac{\varepsilon_{11}^B}{\varepsilon_{11}} \\ Put : \varepsilon_{11}^T = \varepsilon_{11}^I = \varepsilon_{11}^B = \varepsilon_{11} \\ Gives \\ \nu_{12} = \alpha_T.\nu_{12}^T + \alpha_I.\nu_{12}^I + \alpha_B.\nu_{12}^B \\ \nu_{13} = \dfrac{-\varepsilon_{33}}{\varepsilon_{11}} \end{cases} \quad (8)$$

Displacement for 3-direction can be established as:

$$\begin{cases} \delta_3^T = -\nu_{13}^T.\varepsilon_{11}^T.H_T, \quad \delta_3^I = -\nu_{13}^I.\varepsilon_{11}^I.H_I, \quad \delta_3^B = -\nu_{13}^B.\varepsilon_{11}^B.H_B \\ \delta_3 = \delta_3^T + \delta_3^I + \delta_3^B \\ Put\ values = -\nu_{13}^T\varepsilon_{11}^T H_T - \nu_{13}^I\varepsilon_{11}^I H_I - \nu_{13}^B\varepsilon_{11}^B H_B \\ Rewrite : \delta_3 = -\nu_{13}.\varepsilon_{11}.H\ gives \\ -\nu_{13}.\varepsilon_{11}.H = -\nu_{13}^T\varepsilon_{11}^T H_T - \nu_{13}^I\varepsilon_{11}^I H_I - \nu_{13}^B\varepsilon_{11}^B H_B \\ \nu_{13} = -\nu_{13}^T\dfrac{\varepsilon_{11}^T H_T}{\varepsilon_{11}.H} - \nu_{13}^I\dfrac{\varepsilon_{11}^I I}{\varepsilon_{11}.H} - \nu_{13}^B\dfrac{\varepsilon_{11}^B H_B}{\varepsilon_{11}.H} \\ \nu_{13} = \alpha_T.\nu_{13}^T + \alpha_I.\nu_{13}^I + \alpha_B.\nu_{13}^B \\ \nu_{23} = \alpha_T.\nu_{23}^T + \alpha_I.\nu_{23}^I + \alpha_B.\nu_{23}^B \end{cases} \quad (9)$$

2.3 Deformation theory of sandwich beam

This section deals with the elastic analysis of deformation in order to evaluate the stresses in the core or skin and hence the applied loads are corresponding to various failure mechanisms. Considering a simply supported sandwich beam in Fig 7 of span length a, width b and central load p. Each skin has thickness t_f and the two skins are separated by a relatively thick core of thickness, h_c. All layers are perfectly bonded and face material is much stiffer than the core. Considering a higher order shear deformation theory with elastic layers and viscoelastic core, the materials in the core are linear, homogeneous, orthotropic, and made of laminated composite materials. The face layer may be written in the general form:

$$\begin{cases} u^k(x,y,z,t) = u_0^k(x,y,t) + (z-\bar{z}_k)\theta_x^k(x,y,t) \\ w^k(x,y,z,t) = w_0(x,y,z,t) \\ \text{High order deformation Taylor expansion gives} \\ u^c(x,y,z,t) = u_0^c(x,y,t) + z\theta_x^c(x,y,t) + z^2u_0^{*c}(x,y,t) + z^3\theta_x^{*c}(x,y,t) \\ w^c(x,y,z,t) = w_0(x,y,z,t) \end{cases} \quad (10)$$

where u_0^k is the in-plane displacement of the mid-plane of the layer, θ_x^k are rotations of normal, the y-axis (anticlockwise), w_0 is the transverse displacement of the layer, $\bar{z}_k$ is the z coordinate of the mid-plane of each layer, with reference to the core mid-plane ($\bar{z}_c = 0$) and k = t, b is the layer index. For the viscoelastic core layer, applying the high order shear deformation theory, the displacement field is written as second order Taylor series of the in-pane displacements in the thickness coordinate, with constant transverse displacement where u_0^c is the in-plane displacement of the mid-plane of the layer, θ_x^c are rotations of normal to the mid-plane about the y-axis (anticlockwise). The functions u_0^{*c} and θ_x^{*c} are higher-order terms in the series expansion, defined in the mid-plane of the core layer shown in Fig 7 Displacement continuity at interfaces can be written as:

$$\begin{cases} u^c\left(x,y,\frac{h_c}{2},t\right) = u^t\left(x,y,\bar{z}_t-\frac{h_t}{2},t\right) \\ u^c\left(x,y,-\frac{h_c}{2},t\right) = u^b\left(x,y,\bar{z}_b+\frac{h_t}{2},t\right) \\ \text{Coordinates of layer mid-planes} \\ \bar{z}_t = \frac{h_c}{2}+\frac{h_t}{2} \\ \bar{z}_c = 0 \\ \bar{z}_b = -\frac{h_c}{2}-\frac{h_b}{2} \end{cases} \quad (11)$$

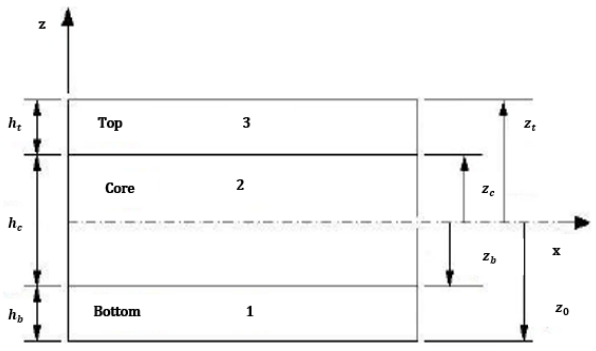

Fig 7: Sandwich beam model

The constitutive relations of the beam model are given as:

$$\begin{cases} \begin{Bmatrix}\sigma_{11}\\ \sigma_{12}\end{Bmatrix}^k = \begin{bmatrix}c_{11} & 0\\ 0 & c_{22}\end{bmatrix}^k \begin{Bmatrix}\epsilon_{11}\\ \epsilon_{12}\end{Bmatrix}^k \\ \text{with} : \\ c_{11} = \frac{E_1}{1-\nu_{12}\nu_{21}}, \quad c_{55} = G_{13} \end{cases} \quad (12)$$

For orthotropic materials, E_1 is in the principal direction {1}, and E_2 is the elasticity modulus in the secondary direction {2}, ν_{12} is Poisson's ratio, whereas: $\nu_{21} = \nu_{12}\frac{E_2}{E_1}$, while G_{13}, G_{23} and G_{12} are the shear moduli for isotropic materials become:

$$\begin{cases} c_{11} = c_{22} = \frac{E}{1-\nu^2} \\ c_{44} = c_{55} = c_{66} \Rightarrow G = \frac{E}{2(1+\nu)} \\ \text{Strain is given by displacement} \\ \begin{Bmatrix}\epsilon_{xx}\\ \epsilon_{xz}\end{Bmatrix}^k = \begin{bmatrix}\frac{\partial}{\partial x} & 0\\ \frac{\partial}{\partial z} & \frac{\partial}{\partial x}\end{bmatrix} \begin{Bmatrix}u\\ w\end{Bmatrix}^k \\ \text{Gives} \\ \epsilon_{xx} = \frac{\partial u_0^c}{\partial x} + z\frac{\partial u_x^c}{\partial x} + z^2\frac{\partial u_0^{*c}}{\partial x} + z^3\frac{\partial \theta_x^{*c}}{\partial x} \\ \gamma_{xx} = \theta_x^c + 2zu_0^{*c} + 3z^2\theta_x^{*c} + \frac{\partial w_0}{\partial x} \end{cases} \quad (13)$$

We obtained the linear strains associated with the for the viscoelastic core layers. Applying the continuity conditions given by (11), one obtains for the top face:

$$\begin{cases} u_0^c + \frac{h_c}{2}\theta_x^c + \frac{h_c^2}{4}u_0^{*c} + \frac{h_c^2}{8}\theta_x^{*c} = u_0^t + \left(z_t - \frac{h_t}{2} - \bar{z}_t\right)\theta_x^t \\ \Rightarrow \\ \theta_x^t = -\frac{2}{h_t}u_0^c + \frac{2}{h_t}u_0^t - \frac{h_c}{h_t}\theta_x^c - \frac{h_c^2}{2h_t}u_x^{*c} - \frac{h_c^2}{4h_t}\theta_x^{*c} \end{cases} \quad (14)$$

and for the bottom face:

$$\begin{cases} u_0^c - \frac{h_c}{2}\theta_x^c + \frac{h_c^2}{4}u_0^{*c} - \frac{h_c^2}{8}\theta_x^{*c} = u_0^b + \left(z_b + \frac{h_t}{2} - \bar{z}_b\right)\theta_x^b \\ \Rightarrow \theta_x^b = \frac{2}{h_b}u_0^c - \frac{2}{h_b}u_0^b - \frac{h_c}{h_b}\theta_x^c + \frac{h_c^2}{2h_b}u_x^{*c} - \frac{h_c^2}{4h_b}\theta_x^{*c} \\ \text{Th strains} : \textit{associated with displacement} \\ \epsilon_{xx}^k = \frac{\partial u_0^k}{\partial x} + z\frac{\partial \theta_x^k}{\partial x} - \bar{z}_k\frac{\partial \theta_x^k}{\partial x} \\ \gamma_{xx}^k = \theta_x^k + \frac{\partial w_0}{\partial x} \end{cases} \quad (15)$$

Considering the rotational restraints between facing beams and core, the distribution of shear stresses t_c is assumed to be uniform through the core depth, h_c. The formula of the mid-span deflection for the sandwich beam in the linear elastic regime as follows:

$$W = \frac{Pa^3}{48E_fI_f} + \frac{Pa}{A_cG_{ca}} \quad (16)$$

where E_f and I_f are modulus of elasticity and moment of inertia of face sheet respectively. While Ac and Gca are cross sectional area of core and average value of elastic shear modulus of the core cell respectively. The first term of the right-hand side in (16) is due to deformation effect alone and the second one account for the shear effect. It is clear that the shear stress related effects brought on by the honeycomb core

cannot be neglected. A simplified formula for predicting the critical value of applied loads is also studied. Considering the assumed stress distribution, the deformation moment of a simply supported honeycomb sandwich beam can be approximately calculated by integrating the first moment of the deformation stress with regard to the neutral axis as follows:

$$\begin{cases} M & = & C.\dfrac{bh^2\sigma_f}{4}\left\{1-\left(\dfrac{h_c}{h}\right)^2\right\} = \dfrac{Pa}{4} \\ C & = & \dfrac{c_1}{c_1+c_2} \\ \text{where} & : & : \\ c_1 & = & \dfrac{a^2}{48E_fE_I} \\ c_2 & = & \dfrac{a}{4A_cG_{ca}} \\ P & = & P_0 \text{Gives} \\ P_0 & = & C.\dfrac{bh^2\sigma_f}{a}\left\{1-\left(\dfrac{h_c}{h}\right)^2\right\} \end{cases} \quad (17)$$

where C is a constant representing the shear effects due to honeycomb core on the resistive deformation moment. The constant C in the above may be obtained by assuming that the shear effects of cores for panel strength are likely to be similar to those for panel stiffness. The critical load in sandwich panel is obtained when the deformation stress of facing reaches the yield stress. Therefore, by in (15) leads us to the critical load P_0.

2.4 The finite element formulation of the orthotropic sandwich beam model

The two transformation methods derived in previous to be evaluated for comparison and possible improvements. This verification is done for two different cases; the beam resting on four supports and the plate working in a full scale model. Both the verification and the parametric study are performed by a finite element simulation (FE). The strength of simulation is that it is a general program which can handle a wide variety of different analysis and simulations. However, in the case of the verification and the parametric study a simple linear analysis will suffice. Appling the principle of minimum potential energy:

$$\begin{cases} \Pi_k & = & U_k + W \\ U_k & = & \frac{1}{2}\int_\Omega \{\epsilon^k\}^T\{\sigma^k\}d\Omega \\ W & = & -\left(\int_\Omega \{d\}^T\{f_b\}d\Omega + \int_S \{d\}^T\{f_S\}dS + \{d\}^T\{f_c\}\right) \\ \{u^k\} & = & [z]^k\{d\} \\ \{d\} & = & \{u_0^c \quad u_0^t \quad u_0^b \quad w_0 \quad \theta_x^c \quad u_0^{*c} \quad \theta_x^{*c}\}^T \\ \{d^e\} & = & \sum_{i=1}^{NN}\{N_i\}\{d_i^e\} = [N]\{a^e\} \end{cases} \quad (18)$$

where Π_k is the potential energy of each layer and U_k and W are, respectively. The energy associated with strains in each layer and the work done by externally applied loads $\epsilon^k$and σ^k are the components of the displacement and tension fields in (18), $\{d\}$, $\{f_b\}$, $\{f_S\}$ and $\{f_c\}$ are the vector of mechanical DOF, the vector of applied loads in the body, the vector of surface tractions and the vector of concentrated forces, respectively. Finally, Ω and S represent volume and surface of domains of the beam, respectively, $[z]^k$ are matrices from obtained from the displacement field of equations in [25]. Integrating in thickness direction (18) and substituting in (17) obtains the variational equation of motion for the sandwich beam, whose solution was obtained through the finite element model using a two-node element with mechanical DOF per node with: N = no of nodes in an element, $N_1 = 1 - \frac{x}{h_e}$, $N_2 = \frac{x}{h_e}$ are the shape functions represented in a matrix [N], h_e is the element length. The strains are related to the B_m, B_b and B_s strain matrices obtained from the shape functions' derivatives:

$$\begin{cases} \{\epsilon_m^e\}^k & = & \sum_{i=1}^{NN}[B_{mi}]^k\{d_i^e\} = [B_m]^k\{a^e\} \\ \{\epsilon_b^e\}^k & = & \sum_{i=1}^{NN}[B_{bi}]^k\{d_i^e\} = [B_b]^k\{a^e\} \\ \{\epsilon_s^e\}^k & = & \sum_{i=1}^{NN}[B_{si}]^k\{d_i^e\} = [B_s]^k\{a^e\} \\ & : & Calculate\ layer-by-layer \\ \{F_u^e\} & = & [K_{uu}^e]\{a^e\} \\ [K_{uu}^e] & = & \sum_{k=c,t,b}\int_{-1}^{1}\left(\begin{matrix}[B_m^e]^T[D_m]^k[B_m^e]^k + [B_b^e]^T[D_c]^k[B_m^e]^k \\ [B_m^e]^T[D_c]^k[B_b^e]^k + [B_b^e]^T[D_b]^k[B_b^e]^k \\ +[B_S^e]^T[D_S]^k[B_S^e]^k\end{matrix}\right)\det[J]d\xi \end{cases} \quad (19)$$

where K is the stiffness matrix of the element, ξ is the neutral coordinate of the element, and J is the Jacobian of the transformation. The $[D_m]$, $[D_c]$, $[D_b]$ and $[D_S]$ are the constitutive matrices with the membrane, coupled, deformation and shear contributions respectively. The following core and facing flexural stiffness formulae:

$$\begin{cases} (EI)_{core} & = & \dfrac{bc^3}{12}E_c \\ I_{face} & = & 2\left[I_{face} + Area\left(\dfrac{d}{2}\right)^2\right] \\ EI & = & \left[\dfrac{bt^3}{6} + \dfrac{btd^2}{2}\right]E_s + \dfrac{bc^3}{12}E_c \\ \delta & = & \dfrac{P(2s^2-3st^2+t^3)}{96EI} + \dfrac{P(S-L)}{4U} \end{cases} \quad (20)$$

The flexural stiffness of core and bottom face materials about M-M axis are calculated from the parallel axis theorem. The ASTM D 7250-06 standard formulae for were applied to calculate flexural stiffness and deflection. The terminology of the terms: EI = Flexural stiffness, b = Width of the specimen, t = Skin thickness, c = Core. Thickness, d = Specimen thickness, Es, Ec = Skin and core Young's Modulus. The other parameters: P = Load applied on the specimen (N), L = Load span length (mm), U = Transverse shear rigidity (M_{Pa}), and S = Support span length (mm).

3. Simulations of the orthotropic sandwich beam model

We develop numerical simulation based on finite-element methods to complement theoretical discussion presented in Section 2 above. We discretized the domain occupied by the problem using different size meshes and implemented procedures and solution algorithms into MATLAB code. We simulated the problem illustrated in Fig 1 under loading in Section 2. For comparison of the errors with the same mesh sizes the beam specimens' characteristics used in Table 1.

Table 1: Specimens' characteristics

Specimens	h_b	h_c	h_t	$\frac{h_c}{h_f}$
	(mm)			
1	12	30	5	3.5
2	12	15	5	1.8
3	12	20	6	2.2
4	12	30	6	3.3
5	10	30	6	3.8

Commonly, the top and bottom face sheets are assigned stiffer properties compared to the core. Engineering constants (3-elastic moduli, 3-Poisson's ratios, and 3-shear moduli) for top-layer, core-layer, and bottom-layer are given in Table 2, Table 3, and Table 4. The comparison of analytical calculated and simulation generated stiffness properties are displayed in the following Table (2-4).

Table 2: Comparison of prescribed and equivalent material property set 1

Initial values, stiffness parameters in (GPa)										
Layer	E_{xx}	E_{yy}	E_{zz}	G_{12}	G_{13}	G_{23}	ν_{xx}	ν_{yy}	ν_{zx}	h(m)
TOP	16.6	9.58	9.58	5.12	4.87	3.72	0.31	0.31	0.29	0.03
CORE	6.55	0.17	5.22	0.483	5.45	0.345	0.33	0.1	0.1	0.19
BOT	12.4	6.21	6.21	3.6	3.38	2.41	0.31	0.29	0.29	0.05
Equivalent properties based on flexural rigidity and axial load-deformation										
Model	E_{xx}	E_{yy}	E_{zz}	G_{12}	G_{13}	G_{23}	ν_{xx}	ν_{yy}	ν_{xx}	h(m)
Rigidity	15.4	6.77	5.93	1.58	4.8	0.27	0.324	0.324	0.466	0.27
L Defl	8.75	2.33	5.93	1.58	4.8	0.27	0.324	0.324	0.466	0.27

Table 3: Comparison of prescribed and equivalent material property set 2

Initial values, stiffness parameters in (GPa)										
Layer	E_{xx}	E_{yy}	E_{zz}	G_{12}	G_{13}	G_{23}	ν_{xx}	ν_{yy}	ν_{zx}	h(m)
TOP	210	210	210	80.7	80.7	80.7	0.3	0.3	0.3	0.03
CORE	0.36	0.36	0.36	0.097	0.097	0.097	0.08	0.08	0.08	0.19
BOT	210	210	210	80.7	80.7	80.7	0.3	0.3	0.3	0.05
Equivalent properties based on flexural rigidity and axial load-deformation										
Model	E_{xx}	E_{yy}	E_{zz}	G_{12}	G_{13}	G_{23}	ν_{xx}	ν_{yy}	ν_{xx}	h(m)
Rigidity	178	178	.511	24.0	0.138	0.138	0.324	0.324	0.466	0.27
L Defl	62.5	62.5	.511	24.0	0.138	0.138	0.324	0.324	0.466	0.27

Table 4: Comparison of prescribed and equivalent material property set 3

Initial values, stiffness parameters in (GPa)										
Layer	E_{xx}	E_{yy}	E_{zz}	G_{12}	G_{13}	G_{23}	ν_{xx}	ν_{yy}	ν_{zx}	h(m)
TOP	100	20	20	5	10.	7	0.2	0.3	0.1	0.03
CORE	2	0.2	5	0.1	0.5	0.3	0.1	0.2	0.1	0.19
BOT	20	100	30	10.	5	7	0.3	0.31	0.29	0.05
Equivalent properties based on flexural rigidity and axial load-deformation										
Model	E_{xx}	E_{yy}	E_{zz}	G_{12}	G_{13}	G_{23}	ν_{xx}	ν_{yy}	ν_{zz}	h(m)
Rigidity	34	26	6.56	2.4	0.687	0.419	0.148	0.232	0.135	0.27
L Defl	16	20	6.56	2.4	0.687	0.419	0.148	0.232	0.135	0.27

The comparison of analytically calculated and simulation generated stiffness properties are made in Table (2-4). To ensure that the chosen materials have realistic behaviour, we also perform check of the load-deformation analysis utilising data in Table (5-7).

Table 5: Top-layer mechanical properties set 1

Face-sheets with stiffer properties compare to the core									
S. No	**Elastic constants (GPa)**						**Poisson's ratios**		
	E_{xx}	E_{yy}	E_{zz}	G_{12}	G_{13}	G_{23}	ν_{xx}	ν_{yy}	ν_{zz}
1	100.6	20.	20.	100.	10	7	0.2	0.3	0.1
2	210.6	210.6e9	210.6	210.6	80.7	80.7	0.3	0.3	0.3
3	100.6	20.e9	20.	100.6	10	7	0.2	0.3	0.1
4	2000.6	1000	500.	2000.6	100	400	0.05	0.06	0.05
5	206	2e	50.	206	3	1	0.15	0.26	0.12
Weaker face-sheets compare to the core									
6	2	5	10	5	0.3	0.1	0.2	0.1	0.3
7	0.2	5	0.3	0.05	0.03	0.01	0.12	0.11	0.23

Table 6: Core-layer mechanical properties set 2

Face-sheets with stiffer properties compare to the core									
S No	**Elastic constants (GPa)**						**Poisson's ratios**		
	E_{xx}	E_{yy}	E_{zz}	G_{12}	G_{13}	G_{23}	ν_{xx}	ν_{yy}	ν_{zz}
1	2	0.2	0.2	0.1	0.5	0.3	0.1	0.2	0.1
2	0.36	0.36	0.36	0.097	0.097	0.097	0.08	0.08	0.08
3	2e9	0.2	0.2	0.1	0.5	0.3	0.1	0.2	0.1
4	0.02	0.04	0.5	0.5	0.9	01	0.1	0.1	0.05
5	0.02	0.046	0.2	0.4	0.09	0.1	0.13	0.22	0.09
	Weaker face-sheets compare to the core								
6	200	100	300	10	0.5	2	0.23	0.12	0.3
7	200	1000	600	100	6	10	0.15	0.12	0.23

Table 7: Bottom-layer mechanical properties set 3

S. No	E_{xx}	E_{yy}	E_{zz}	G_{12}	G_{13}	G_{23}	ν_{xx}	ν_{yy}	ν_{zz}
1	210.4	210.4	210.4	80.7	80.7	80.7	0.3	.3	0.3
2	20.4	100.4	100.4	10.	5	7	0.3	.31	0.29
3	20.4	100.4	100.4	10.	5	7	0.3	.31	0.29
4	400	200	40	50.	53	71	0.1	.1	0.29
5	15	40	1	2.	3	24	0.15	.11	0.15
	Weaker face-sheets compare to the core								
6	10	20	2	5	1	5	0.12	.15	0.2
7	1e	2	22	0.5	10	1	0.17	.14	0.15

4. Results and Discussions

The simulation performed to find a relation between E_{11} and E_{22} that minimized the deformation. For evenly distributed load where magnitude only scales the deflection and thus have no influence on the ratios between the two stiffness as E_{11} was fixed and E_{22} were varied in intervals. The affected shear moduli in the different directions were calculated and set to obtain full linear strain according to the equations derived from the study. For every material set the largest deflection was measured and plotted together with E_{11} and E_{22} which formed a surface plot as seen in Fig 8.

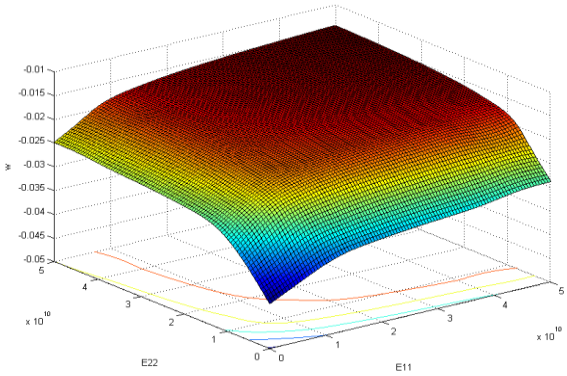

Fig 8: Surface plot of E_{11}, E_{22} and displacement w.

The simulated results are compared to the problem results available in the literature to quantify properties and suitability for a specific structural problem. It is evident from plot of the figure simulated results commute satisfactorily. The simulation generated data results by the axial-compression and flexural methods, the deflection quantities U_3 are plotted against reference quantities in x-directions. Comparisons of the deflection quantities by axial-compressive and flexural methods against referred method for input data set 1 and set 2 are plotted in Fig 9 and Fig 10 respectively. Comparison of flexural and referred curves illustrate slight different but similar downward trend. Nonetheless, it can be seen that the deflection curve representing axial-compressive quantities

show much more deflection when compared to the flexural and referred curves. This predicts a situation may have occurred where extensional moduli E_{11} and E_{22} for a certain allowed deflection were not stiff enough, and result in a larger deflection (outlier). Comparisons of the deflection quantities by axial-compressive and flexural methods against referred method for input data sets 3 are plotted in Fig 11.

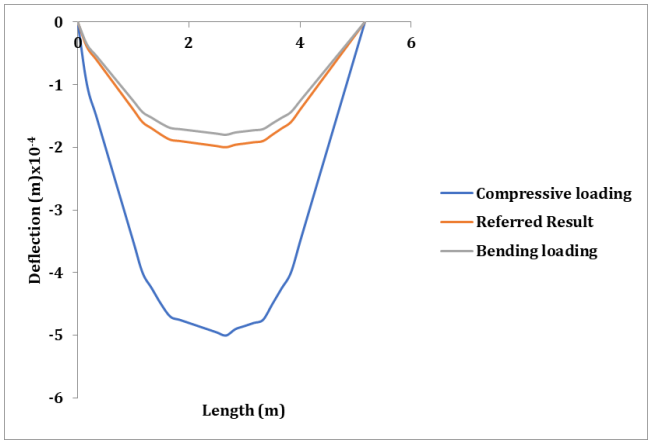

Fig 9: Deflection U3 along x-direction for parameter set 1

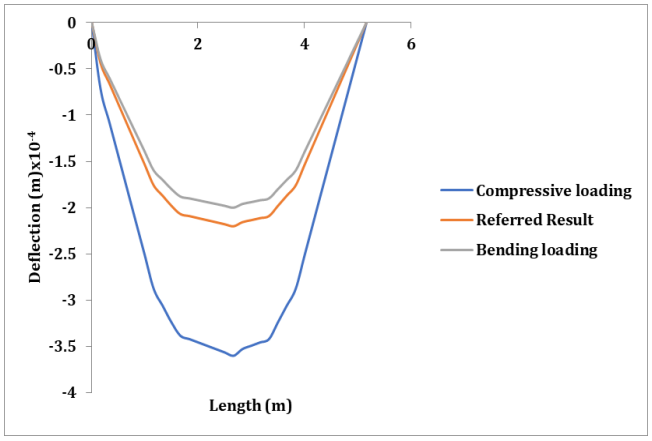

Fig 10: Deflection U3 along x-direction for parameter set 2.

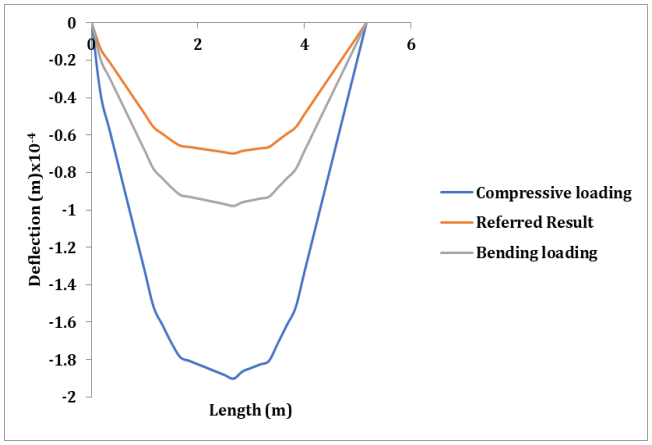

Fig 11: Deflection U3 along x-direction for parameter set 3

It was observed that the elastic, shear moduli, and Poisson's ratios quantities agree well with referred quantities depicted in the tables. The shear transformation methods are normally verified by comparison of the deflection. Since deformation is a combination of deformation and shear, and contributes much more to the total deflection compared to shear.

The graphical visualisation of computer simulations generated data by axial-compressive and flexural methods for both the realistic and un-realistic data cases exhibit similar trends. The data quantities illustrated are according to the expectation. Intra comparison of the flexural and compression transformation gives that flexural results are more accurate result than the axial-compressive ones. These may affect the ratio between E_{11} and E_{22} by having localized maximum deflections in different points depending on the load case, which will lead to a more complicated relation obtained by the ratios between the elastic and shear moduli. These ratios are also affected by the loading when measuring the strains, for instance if strain ϵ_{11} is not be symmetrical over the width of the beam and changes under loading which makes the expression regarding G_{12} hard to approximate. This also applies for the strain ϵ_{22} which makes the ratio between E_{22} and G_{23} dependent on the loading conditions.

5. Conclusions

Analytical and simulation analyses of orthotropic sandwich beams were performed with approximated effective engineering constants under axial-compressive and flexural deformation loading. Overall the transformation based on constant flexural rigidity method seems to have better correlation, more stable, and varying not much between the different parameter sets than the other axial deformation and referred methods. Comparisons of the selected results to the data results available in literature were found to be within the acceptable agreement up to (±6%) deviations. The developed simulation model of hybrid orthotropic sandwich beams has reliably evaluated material properties by transforming multi-layer heterogeneous sandwich beam into an equivalent one layer beam as well as deformation behaviour under axial and bending combined loadings. The proposed simulation model is economical, efficient, and reliable. Therefore, the proposed study is recommended for similar future investigations and analyses of the commercial products, structural assets, and to present possible improvements.

6. References

1. Rayjade GR, *et al*. Study of sandwich structure and deformation characteristics: A review. International Journal of Current Engineering and Technology. 2015; 5(2).
2. Jamal Arbaoui, Yves Schmitt, J-Luc Pierrot, Francois-Xavier Royer. Numerical Simulation and Experimental Deformation Behaviour of Multi-Layer Sandwich Structures Journal of Theoretical and Applied Mechanics. 2014; 52(2):431-442.
3. Kantha Rao K, Jayathirtha Rao K, Sarwade AG, Madhava Varma B. Deformation Behavior of Aluminum Honey Comb Sandwich Panels International Journal of Engineering and Advanced Technology. 2012; 1(4):268-272.
4. Kantha Rao K, Jayathirtha Rao K, Sarwade AG. Strength Analysis on Honeycomb Sandwich Panels of different Materials International Journal of Engineering Research and Applications. 2012; 2(3):365-374.
5. Abaqus. Abaqus Cae 6.13 user's guide. RI, USA: Dassault Systèmes Simulia Corp, 2013.
6. Dai GM, Zhang WH. Size effects of basic cell in static analysis of sandwich beams International Journal of Solids and Structures. 2008; 45:2512-2533.

7. Venugopal MM, Maharana SK, Badarinarayan KS. Finite Element Evaluation of Composite Sandwich Panel under Static Four Point Deformation Load, JEST. 2013; 2(1):1-6.
8. Araújo AL, Mota Soares CM, Mota Soares CA. Finite Element Model for Hybrid Active-Passive Damping Analysis of Anisotropic Laminated Sandwich Structures. Journal of Sandwich Structures and Materials. 2010; 12:397-419.
9. Reddy JN. Mechanics of Laminated Composite Beams and Shells: Theory and Analysis, 2nd Edition, CRC Press, Boca Raton, USA, 2004.
10. San HaN, Lu G. A review of recent research on bio-inspired structures and materials for energy absorption applications. Compos B Eng. 2020; 181:107496.
11. Yang P, Shams S-S, Slay A, Brokate B, Elhajjar R. Evaluation of temperature effects on low velocity impact damage in composite sandwich panels with polymeric foam cores. Compos Struct. 2015; 129:213-223.
12. Liu J, He W, Xie D, Tao B. The effect of impactor shape on the low-velocity impact behaviour of hybrid corrugated core sandwich structures. Compos B Eng. 2017; 111:315-331.
13. He W, Lu S, Yi K, Wang S, Sun G, Hu Z. Residual flexural properties of CFRP sandwich structures with Aluminium honeycomb cores after low-velocity impact. Int J Mech Sci. 2019; 161:105026.
14. Meram A, Cetin ME. Experimental investigation on the effects of core/facing interface performance on the low-velocity impact behaviour of honeycomb sandwich panels. J Mater Eng Perform. 2020; 29(11):7408-7419.
15. Xiao Y, Jiang D. Rate dependence of transformation pattern in super elastic NiTi tube. Extreme Mech Lett. 2020; 39:100819.
16. Xiao Y, Jiang D. Constitutive modelling of transformation pattern in super elastic NiTi shape memory alloy under cyclic loading. Int J Mech Sci. 2020; 182:105743.
17. Shanyouming Sun, Dan Liu, Yinglong Sheng, Shang sheng Feng, Hongbin Zhu, Tian Jian Lu. Out-of-plane compression of a novel hybrid corrugated core sandwich panel. Composite Structures (Elsevier), 2021.
18. Clément Audibert, Anne-Sophie Andréani, Éric Lainé, Jean-Claude Grandidier. Discrete modelling of low-velocity impact on Nomex® honeycomb sandwich structures with CFRP skins. Composite Structures (Elsevier), 2019.
19. Junhua Zhang, Xiufang Zhu, Xiaodong Yang, Wei Zhang. Transient Nonlinear Responses of an Auxetic Honeycomb Sandwich Beam under Impact Loads. International Journal of Impact Engineering, 2019.
20. Anil Kumar, Arindam Kumar Chanda, Surjit Angra. Numerical Modelling of a Composite Sandwich Structure Having Non-Metallic Honeycomb Core. Evergreen Joint Journal of Novel Carbon Resource Sciences & Green Asia Strategy. 2021; 8(4):759-767.
21. Kiran Kumar Reddy Y, Reddy NV. Design and Analysis of Sandwich Honey Comb Structures. International Journal of Research in Engineering, Science and Management. 2019; 2(1).
22. Saiaf Bin Rayhan, Mahtab Uddin Chowdhury, Xue Pu. Ballistic impact response of reinforced honeycomb sandwich panels. IOP Conf. Series: Materials Science and Engineering, 2022.
23. Tarlochan F. Sandwich structures for energy absorption applications: A review. Materials, 2021. Doi: https:// doi. org/ 10. 3390/ ma14164731
24. Ahmed S, Galal K. Response of metallic sandwich panels to blast loads. J Struct Eng. 2019; 1:21. Doi: https:// doi. org/ 10. 1061/ (ASCE) ST. 1943- 541X. 00023 97.
25. Luo F, Zhang S, Yang D. Anti-explosion performance of composite blast wall with an Auxetic re-entrant honeycomb core for offshore platforms. J Mar Sci Eng, 2020. Doi: https:// doi. org/ 10.3390/ jmse8 030182.
26. Qi C, Remennikov A, Pei L-Z, Yang S, Yu Z-H, Ngo TD. Impact and close-in blast response of auxetic honeycomb-cored sandwich panels: experimental tests and numerical simulations. Compos Struct, 2017. Doi: https:// doi. org/ 10. 1016/j. comps Struct. 2017. 08.020
27. Li J, Shi S, Luo W, Wang Q. Study on explosion-resistance of Biomimetic layered honeycomb structure. Adv Civ Eng, 2020. Doi: https:// doi. org/ 10. 1155/ 2020/ 53561 45
28. Imbalzano G, Linforth S, Ngo TD, Lee PV, Tran P. Blastresistance of auxetic and honeycomb sandwich panels: Comparisons and designs. Compos Struct, 2017. Doi: https:// doi. org/ 10. 1016/j. comps truct. 2017. 03. 018
29. Al-Rifaie H, Studzinski R, Gajewski T, Malendowski M, Sumelka W, Sielicki PW. A new blast absorbing sandwich panel with unconnected corrugated layers-numerical study. Energies, 2021. Doi: https:// doi. org/ 10. 3390/ en140 10214